frontiers | Frontiers in Marine Science

TYPE Original Research
PUBLISHED 22 November 2024
DOI 10.3389/fmars.2024.1497360



OPEN ACCESS

EDITED BY
Travis Blake Meador,
Academy of Sciences of the Czech Republic (ASCR), Czechia

REVIEWED BY
Frank Dehairs,
Vrije University Brussels, Belgium
Wangwang Ye,
State Oceanic Administration, China

*CORRESPONDENCE
Sofia Muller
sofiamuller.be@hotmail.com;
sofia.muller@uliege.be
Bruno Delille
bruno.delille@uliege.be

RECEIVED 16 September 2024
ACCEPTED 28 October 2024
PUBLISHED 22 November 2024

CITATION
Muller S, Fripiat F, Jaccard SL, Ponsoni L, Hölemann JA, Martínez-García A and Delille B (2024) Nitrous oxide dynamics in the Kara Sea, Arctic Ocean.
*Front. Mar. Sci.* 11:1497360.
doi: 10.3389/fmars.2024.1497360



# Nitrous oxide dynamics in the Kara Sea, Arctic Ocean

Sofia Muller[1,2,3]*, François Fripiat[2], Samuel L. Jaccard[4], Leandro Ponsoni[5], Jens A. Hölemann[6], Alfredo Martínez-García[3] and Bruno Delille[1]*

[1]Unité d'Océanographie Chimique, Université de Liège, Liège, Belgium, [2]Department of Geosciences, Environment and Society, Université Libre de Bruxelles, Bruxelles, Belgium, [3]Organic Isotope Geochemistry group, Max Planck Institute for Chemistry, Mainz, Germany, [4]Institute of Earth Sciences, University of Lausanne, Lausanne, Switzerland, [5]Flanders Marine Institute (VLIZ), Oostende, Belgium, [6]Alfred Wegener Institute, Helmholtz Centre for Polar and Marine Research, Bremerhaven, Germany

Previous studies have reported an accumulation of nitrous oxide ($N_2O$) on shallow continental shelves of the western Arctic Ocean. In this study, we sampled seawater profiles for $N_2O$ measurements in the eastern Arctic shelves, in the North Kara Sea, in the context of the Arctic Century Expedition. Despite some variability in the vertical distribution, we typically observe an accumulation of $N_2O$ in shelf bottom waters, which correlates with a fixed nitrogen (N) deficit. Longer residence times on the shelf promote greater $N_2O$ enrichment and a larger fixed N deficit. These observations point towards $N_2O$ production at depth, linked to benthic denitrification processes that are intensified on productive shelve areas. However, in surface waters, physical processes – i.e. temperature-dependent solubility and air-sea exchange – emerge as the main factor controlling $N_2O$ concentrations. We observe low saturations of 80% at the surface of open ocean stations influenced by water that has previously flowed beneath sea ice. Arctic surface water becomes undersaturated due to cooling and remains undersaturated due to limited air-sea exchange. River supply does not exert a discernable influence on $N_2O$ concentrations of the studied area. This study reveals the potential of the Arctic Siberian shelves as a sink of atmospheric $N_2O$ during the summer.

KEYWORDS

**nitrous oxide, $N_2O$ flux, air-sea exchange, Kara Sea, arctic ocean, nitrification, denitrification, nitrogen cycle**

## 1 Introduction

Nitrous oxide ($N_2O$) is a potent greenhouse gas (IPCC, 2023), and is the dominant ozone-depleting substance in the stratosphere (Ravishankara et al., 2009). $N_2O$ atmospheric concentrations have increased by > 23% since 1750, with a significant increase in the last 4 decades (IPCC, 2023). Anthropogenic $N_2O$ sources account for one

third of the total emissions, but are the primary drivers of the observed increase in atmospheric $N_2O$ levels (Tian et al., 2024). Oceans naturally emit 4.7 Tg N $y^{-1}$, which represents 26% of the total $N_2O$ emissions (or 40% of the natural emissions) (Tian et al., 2024). Oceanic $N_2O$ emissions predominantly occur in the tropics and in coastal upwelling systems (Yang et al., 2020). More accurate estimates of $N_2O$ emissions from ocean sources and their response to climate change, are hindered by a general lack of observational data from large areas of the ocean, in particular polar environments (Yang et al., 2020; Tian et al., 2024).

$N_2O$ is primarily produced via two microbial processes, namely nitrification and denitrification. These two processes are inherently linked to the production and remineralization of organic matter, and nitrogen cycling. Nitrification is a type of chemoautotrophy that takes place when ammonium ($NH_4^+$) is released during the decomposition of organic matter (Ward, 2008; Tang et al., 2023). It is the aerobic, two-step oxidation of ammonium ($NH_4^+$) to nitrite ($NO_2^-$) and then nitrate ($NO_3^-$). $N_2O$ is considered as a by-product of the oxidation of $NH_4^+$ to $NO_2^-$. The positive correlation between apparent oxygen utilization (AOU) and $N_2O$ concentration anomalies (i.e., $\Delta N_2O$) suggests that most of the $N_2O$ in the ocean is produced by nitrification processes (Cohen and Gordon, 1979; Bange, 2008). Denitrification, on the other hand, takes place under anaerobic conditions. Denitrification relates to the reduction of $NO_3^-$ to dinitrogen ($N_2$), with $N_2O$ being both, a product and an intermediate reactant of the reaction chain (Bothe et al., 2000). Denitrification is the major sink of fixed nitrogen (N) in the ocean by converting fixed N to $N_2$ (Brandes and Devol, 2002; Bianchi et al., 2012).

Continental shelve regions represent an important source of $N_2O$ to the atmosphere. They represent 9% of the total ocean area (Harris et al., 2014) but contribute to 1.2 Tg N $y^{-1}$ – i.e., 26% of the oceanic $N_2O$ emissions – to the atmosphere (Tian et al., 2024). According to global models, a large fraction of the denitrification occurs in continental shelf sediments (Seitzinger et al., 2006), where sedimentary organic carbon flux is highest (Bianchi et al., 2012) and pelagic and benthic processes are tightly coupled (Rowe et al., 1975; Sun et al., 2021). Therefore, continental shelves represent a major sink of fixed N, and a potentially important source of $N_2O$ to the atmosphere (Tian et al., 2024).

Half of the Arctic Ocean is characterized by vast, shallow shelf areas (Harris et al., 2014). It is estimated that the Arctic continental shelves account for 4% to 13% of the fixed N loss from the ocean (Devol et al., 1997; Chang and Devol, 2009; McTigue et al., 2016). Most studies, reporting $N_2O$ concentrations, are localized in the western Arctic Ocean (Hirota et al., 2009; Kitidis et al., 2010; Zhan et al., 2015, 2021; Zhang et al., 2015; Fenwick et al., 2017; Wu et al., 2017; Heo et al., 2021; Toyoda et al., 2021; Liu et al., 2022, 2024; Manning et al., 2022; Schuler and Tortell, 2023), and data from the eastern Arctic Ocean remain scarce. Observations suggest that benthic denitrification is the main process leading to $N_2O$ production over the shelves (Hirota et al., 2009; Zhan et al., 2015; Fenwick et al., 2017; Toyoda et al., 2021; Manning et al., 2022), while the observed concentrations in the intermediate and deep waters of the Arctic Ocean typically relate to a combination of nitrification and poor-ventilation rates of the Arctic waters that were exposed to past atmospheric concentrations (Zhang et al., 2015; Zhan et al., 2016; Fenwick et al., 2017; Heo et al., 2021; Toyoda et al., 2021). To the best of our knowledge, Wild et al. (2023) is the sole study reporting $N_2O$ concentrations in the eastern Arctic. They reported aerobic or anoxic $N_2O$ consumption in the water column or in particle microsites, respectively, rather than a sedimentary source.

Rivers contribute to a large amount of organic material and land-derived nutrient input (Opsahl et al., 1999; Holmes et al., 2012; McClelland et al., 2016), sustaining potentially one third of the annual primary production in the Arctic Ocean (Terhaar et al., 2021). The Kara Sea receives substantial river discharge accounting for more than one third of the total riverine freshwater input to the Arctic Ocean (Aagaard and Carmack, 1989). The West Siberian lowlands contain the most extensive peatlands and substantial fraction of the global terrestrial carbon stocks (Sheng et al., 2004; Smith et al., 2004). Arctic warming accelerates permafrost thaw and is expected to promote higher inputs of particulate and dissolved nitrogen from rivers into the ocean (Frey et al., 2007). Land-derived nitrogen input can serve as a substrate for the marine nitrogen cycle, potentially enhancing biogeochemical processes and contributing to increased $N_2O$ production.

In the present study, we provide full-depth water column profiles of $N_2O$ in the northern Kara Sea. The samples were collected in summer during the sea-ice melting season, in the context of the Arctic Century Expedition. $N_2O$ shows heterogenous concentrations, with contrasting results between open ocean and shelves areas, or between ice-free and ice-covered stations, underscoring the importance of water circulation and provenance on $N_2O$ inventories. We show that shelf bottom waters are enriched in $N_2O$, likely due to benthic denitrification, while surface waters are near equilibrium with the atmosphere with $N_2O$ concentrations primarily being regulated by sea water temperature. This contrasts with ~80% saturation observed in surface waters of open ocean area, influenced by water that had previously flowed beneath sea ice. This undersaturation is likely driven by combination of cooling, limited air-sea exchange, and vertical mixing with deeper undersaturated water masses.

# 2 Materials and methods

## 2.1 Study site

The Kara Sea, like most eastern Arctic marginal seas, is distinguished by its extensive and shallow continental shelf, and is seasonally covered by sea ice (Figures 1, 2). Perpendicular to the shelf break, the continental shelf exhibits two distinct troughs: the St. Anna Trough to the west, reaching a maximum depth of 620 m, and the Voronin Trough to the east, with a maximum depth of 450 m (Figure 1). The overall circulation in the Kara Sea is characterized by a semi-cyclonic pattern. Waters of Atlantic origin enter the Kara Sea via the Fram Strait Branch Water (FSBW) from the northwestern side of the St. Anna Trough, flowing southwards. Simultaneously, the Barents Sea Branch Water (BSBW) enters the western side of the St. Anna Trough, flowing northwards (Figure 1).

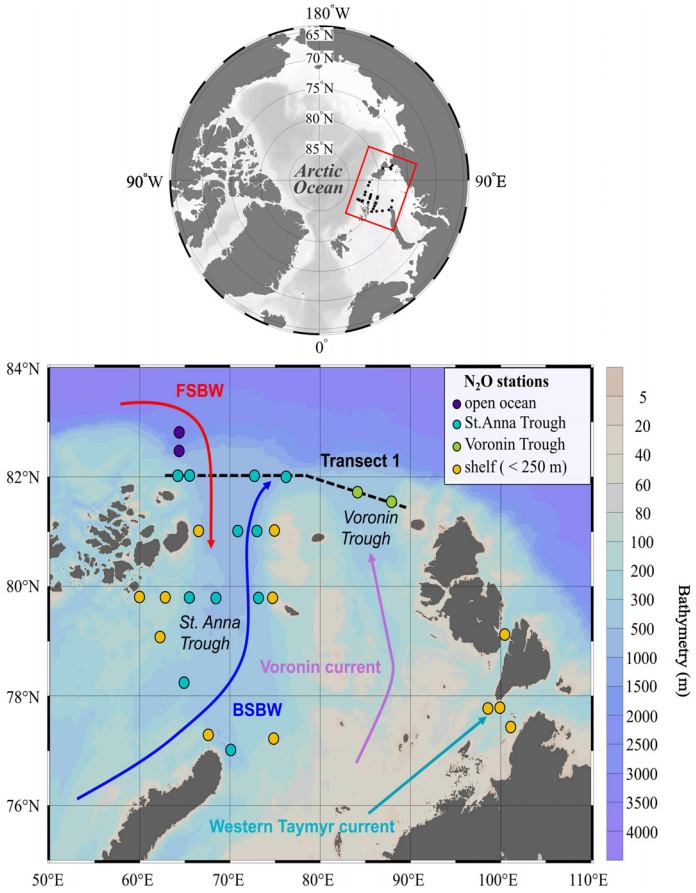


FIGURE 1
$N_2O$ sampling stations in circles, categorized by location and depth. Open ocean stations (in dark blue) are beyond the continental shelf (>2000 m depth), shallow shelf stations (in yellow) have a depth <250 m, and St. Anna (in light blue) and Voronin Trough stations (in green) are on the continental shelf (>250 m depth). Water circulation is indicated by colored arrays representing the Fram Strait Branch Water (FSBW), the Barents Sea Branch Water (BSBW), the Western Taymyr and the Voronin current. This circulation is further supported by the geostrophic current field shown in Figure 2. Squares on transect 1 represent additional profiles of temperature (white squares) and nutrients (black filled squares).

The area also receives substantial river discharge from the Ob and Yenisei, accounting for approximately 40% of the total river runoff in the Arctic Ocean (Aagaard and Carmack, 1989; Makkaveev et al., 2015). The resulting river plume typically flows eastward along the Siberian coast (Figure 1) (Janout et al., 2020).

## 2.2 Sampling

Samples were collected as part of the Arctic Century Expedition, which took place from August 5$^{th}$ to September 6$^{th}$, 2021, aboard RV *Akademik Tryoshnikov*. A total of 27 stations were sampled for full-depth profile measurements of $N_2O$ concentrations (Figure 1).

During the expedition, physical and biogeochemical properties were also investigated, including salinity, temperature, nutrient, and dissolved oxygen ($O_2$) concentrations. Salinity and temperature data were collected using a CTD equipped with sensors for conductivity, temperature, and pressure (SBE911+) as described in Hölemann et al. (2022) and (Gangnus et al., 2022) for water bottle samples. To determine the mixed layer depth, we employed the threshold method with a finite-density difference criterion (0.03 kg m$^{-3}$) relative to a near-surface reference value (de Boyer Montégut et al., 2004). Dissolved $O_2$ was measured onboard via a standard Winkler titration using a Metrohm 916 TiTouch automatic titrator and handheld titrator (BRAND1) (Gangnus et al., 2022). Samples for nutrient analysis were stored frozen (-20°C) in MQ-cleaned HDPE 60ml bottles until their analysis at MPIC. Nutrient concentration (nitrate, $NO_3^-$, nitrite, $NO_2^-$, ammonium, $NH_4^+$, and phosphate, $PO_4^{3-}$) were measured using standard colorimetric methods (Hydes et al., 2010) on board for $NH_4^+$ (Gangnus et al., 2022) and in home laboratory on frozen sample for $NO_3^-$, $NO_2^-$, $PO_4^{3-}$ (Muller et al., 2024). We used N* concentration to estimate the deficit in fixed N (i.e., biologically available nitrogen) in comparison to phosphate, according to N* = DIN – 16 * $PO_4^{3-}$ + 2.9 (Gruber and Sarmiento, 1997), with DIN (i.e., dissolved inorganic nitrogen) = $NO_3^-$ + $NO_2^-$ + $NH_4^+$.

## 2.3 $N_2O$ concentration

$N_2O$ samples were collected from the Niskin bottles using a Tygon® tube and transferred into borosilicate 60 ml serum bottles.

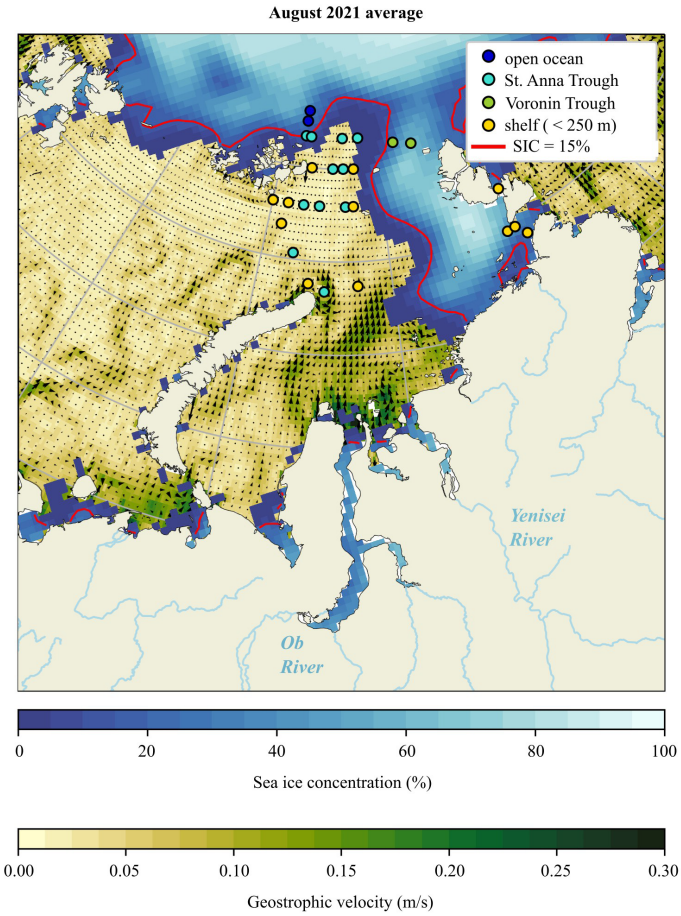


FIGURE 2
Sea surface current. Monthly average of the geostrophic velocity and the sea ice concentration for August 2021. Data is available on the Copernicus Marine Service for geostrophic velocity (doi:10.48670/moi-00145) and sea ice concentration (doi: 10.48670/moi-00136).

Samples were poisoned by introducing 60 µL saturated mercury chloride ($HgCl_2$) solution. The bottles were sealed with isobutyl stoppers and securely capped with aluminum crimps. The bottles were then kept in the dark at room temperature until analysis at home laboratory. Measurements of $N_2O$ concentration (Muller et al., 2024) were conducted using the headspace technique described by Weiss (1981) and Upstill-Goddard et al. (1996). Briefly, approximately 25 mL of the sea water sample was replaced by ultra-pure N gas (AirLiquide Belgium®, Alphagaz 2, $N_2 \geq 99.9999\%$), followed by manual agitation and overnight equilibration in a water bath at room temperature. A 12 mL extraction from the headspace was injected into an SRI Instrument Model 8610C Gas Chromatograph with Electron Capture Detector, for analysis. The calibration was performed using precision gas mixtures containing $N_2O$, $CH_4$, $CO_2$, and $N_2$, provided by AirLiquide Belgium®. These calibration standards bracketed the sample concentrations, with a mixing ratio of 0.19 ± 0.02 ppm and 0.94 ± 0.09 ppm. Measurements derived from a 12-replicate-sampling of Arctic waters showed a precision of ± 0.5 nM (1σ) and ± 4% (1 relative standard deviation). The accuracy of the ECD was tested using an internal standard with a $N_2O$ concentration of 0.55 ± 0.09 ppm (Air Liquide) and we report a difference of 3% with the certified value which is within the bracketed error of the internal standard (that is at 10%).

The $N_2O$ saturation is estimated using the following equation:

$$N_2O \text{ saturation } (\%) = \frac{C_{ob}}{C_{eq}} \times 100 \quad (1)$$

where $C_{obs}$ represents the observed concentration of $N_2O$, while $C_{eq}$ represents the theoretical equilibrium concentration of $N_2O$ in sea water. The determination of the latter is conducted through the application of the Henry's Law, as formulated by Weiss and Price (1980), to compute the equilibrium concentration of $N_2O$, based on the specific temperature and salinity of sea water (i.e., the solubility of $N_2O$ in seawater). The mean atmospheric $N_2O$ mixing ratios were obtained from the discrete dataset at Ny-Alesund (ZUP), Svalbard – from July 1$^{st}$, 2021 to September 30$^{th}$, 2021 (NOAA 2024). Error propagation, considering the precision in $N_2O$ concentration measurements, results in a standard deviation of 3% for $N_2O$ saturation (1σ).

The $N_2O$ concentration anomaly ($\Delta N_2O$) was calculated using the following equation:

$$\Delta N_2O = C_{ob} - C_{eq} \quad (2)$$

## 2.4 Air-sea fluxes

Sea-air flux calculation was performed using the gas transfer velocity parametrization of Ho et al. (2006), with Schmidt numbers for $N_2O$ following Wanninkhof (2014). Positive values represent a flux from the sea to the air (source) and negative values a flux from the air to the sea (sink). *In situ* wind speed was measured aboard R/V *Akademik Tryoshnikov* with two 2-D sonic anemometers (models W S425 and WMT702), which were operated as part of an automated weather station (AWS; model AWS420, Vaisala) (Thurnherr et al., 2024). Wind speeds were converted from 30 m to 10 m height using the equation from Hsu et al. (1994):

$$u_{30} = u_{10}\left(\frac{10}{30}\right)^{0.11} \quad (3)$$

A correction factor was added to areas partially covered by sea ice. Sea-air flux estimates were scaled to the fraction of open water within the sea ice area (Butterworth and Miller, 2016):

$$F = (1 - f_{ice})\, K_{coeff}\, \Delta pN_2O_{sw-atm} \quad (4)$$

where $f_{ice}$ is the sea ice fraction derived from OSI SAF (doi: 10.48670/moi-00136), $K_{coeff}$ is the gas transfer velocity, and $\Delta pN_2O$ is the partial pressure difference between the seawater and the atmosphere.

## 2.5 Satellite-based datasets

This study uses daily satellite-based absolute geostrophic velocity fields, gridded onto a regular 0.25° × 0.25° grid. The data product 'Global Ocean Gridded L 4 Sea Surface Heights And Derived Variables Reprocessed Copernicus Climate Service', is produced and provided by the Copernicus Climate Change Service (C3S). The geostrophic velocities are derived from altimetry sea level records obtained from a stable two-satellite constellation, ensuring the stability and homogeneity of the dataset (doi:10.48670/moi-00145). For the period of the cruise, monthly means were calculated from the daily data (Figure 2).

In addition, satellite-based daily sea ice concentration fields provided by the European Organization for the Exploitation of Meteorological Satellites (EUMETSAT) are incorporated in this study (Figure 2). Specifically, the OSI-430-a product produced by the Ocean and Sea Ice Satellite Application Facility (OSI SAF), covering the period from 2021 to the present. This product calculates sea ice concentration using atmospherically corrected Passive Microwave (PMW) brightness temperatures derived from the Scanning Multichannel Microwave Radiometer (SMMR), Special Sensor Microwave/Imager (SSM/I), and Special Sensor Microwave Imager/Sounder (SSMIS). The data, classified as Level 4 and gridded at a spatial resolution of 25 × 25 km, are accessible via the Copernicus Marine Service (CMEMS) under the full title 'Global Ocean Sea Ice Concentration Time Series REPROCESSED (OSI-SAF)' doi: 10.48670/moi-00136).

Furthermore, this study utilizes daily sea surface salinity (SSS) and sea surface temperature (SST) data from the TOPAZ5 Arctic Ocean reanalysis system. The TOPAZ5 product, identified as 'Arctic Ocean Physics Analysis and Forecast' (doi:10.48670/moi-00016), is provided by the CMEMS. The operational TOPAZ5 system employs the HYCOM model and a 100-member Ensemble Kalman Filter (EnKF) assimilation scheme. The TOPAZ5 product for SSS and SST has a spatial resolution of 6 x 6 km.

# 3 Results

## 3.1 $N_2O$ concentration

Sea water $N_2O$ concentrations in the Kara Sea typically ranged from 11.1 nM to 18.5 nM, with a mean concentration of 15.1 ± 1.3 nM (Figure 3A). Despite the heterogeneity of the data, a clear pattern emerged when the stations were categorized based on their location and depth (Figures 1, 3A). We designated stations beyond the continental shelf break (> 2000 m depth) as open ocean stations (n = 2; blue circles in Figure 1). Over the shelf area, a further distinction was made between shallow shelf stations (< 250 m; n = 12; yellow circles) and those located in the St. Anna Trough (n = 11; cyan circles) and Voronin Trough (n = 2; green circles), at > 250 m.

Overall, averaged $N_2O$ concentrations profiles increased from the open ocean to the shelf stations (Figure 3A). The highest concentrations were observed in the Voronin Trough, followed by the shallow shelf, with the St. Anna Trough stations exhibiting values slightly higher than those of the open ocean stations. Vertical profiles revealed a consistent rise in $N_2O$ concentration towards the bottom, with the exception of the Voronin Trough, which showed relatively constant yet higher concentrations throughout the entire water column. The increase in $N_2O$ concentrations at depth was more pronounced for the shelf stations (<250 m). However, a large scattering appeared between stations (Supplementary Figure S1) with 2 stations showing a decrease in $N_2O$ concentration with depth (stations 32 and 41; S1), 8 stations showing similar $N_2O$ concentration with depth (stations 17, 26, 38, 40, 59, 104, 109, 111) and 17 stations showing an increase in $N_2O$ concentration with depth (all the other stations). Both, the St. Anna Trough and the shallow shelf exhibited surface concentrations of 14.0 nM to 15.0 nM, as the open ocean, whereas the surface in the Voronin Trough showed $N_2O$ concentrations of 17.3 nM, i.e., in the same concentration range than shelf bottom water. Such distribution was further illustrated with one transect, located at the northern continental shelf break (Figure 4 and dashed black line in Figure 1), showing a contrast between the two throughs: $N_2O$ concentrations were higher in the Voronin Trough. In parallel to these variations in $N_2O$ concentrations, lower DIN concentrations and lower $N^*$ (i.e., higher deficit in N relative to P) concentrations appeared over the shelves and the Voronin Trough compared to the St. Anna Trough and the open ocean (Figures 3C, D).

## 3.2 $N_2O$ saturation

$N_2O$ saturations within the mixed layer ranged from 78% to 111%, with a mean value of 95 ± 6% (Figure 3B). When considering the entire water column, the saturation levels ranged from 70% to

116%, with an average of 95 ± 7% (Figure 3B). The Voronin Trough exhibited a less variable profile that is oversaturated throughout the entire water column. In contrast, the shelves were undersaturated at the surface (96%), similar to the St. Anna Trough, and transition to oversaturation levels like the Voronin Trough at bottom depth (103%). The saturations levels for the St. Anna Trough first decreased, reaching levels similar to the open ocean (~90%) at a depth of 75m, and then slightly increased with depth, following the trend observed in the open ocean. The open ocean and St. Anna Trough were undersaturated along the entire water column. By contrast to all mean profiles, the open ocean revealed a saturation decrease near surface waters, and the strongest undersaturation, with a mean value of 83%.

## 3.3 $N_2O$ sea-air fluxes

We calculated the sea-air fluxes across the northern Kara Sea (Table 1). We further distinguished the ice-free area and the off-shelf area that shows the strongest $\Delta N_2O$ gradient. Fluxes for the entire Kara Sea ranged from -4.0 µmol $N_2O$ $m^{-2}$ $d^{-1}$ to 1.8 µmol $N_2O$ $m^{-2}$ $d^{-1}$ with a mean and standard deviation of -0.6 ± 1.0 µmol $N_2O$ $m^{-2}$ $d^{-1}$, suggesting a minor sink for the area during summertime. Off-shelf area displayed a stronger sink with a mean value of -2.9 ± 1.5 µmol $N_2O$ $m^{-2}$ $d^{-1}$, despite the partial presence of sea ice, largely due to the strong saturation gradient between seawater and the atmosphere.

# 4 Discussion

## 4.1 $N_2O$ production over the bottom waters of the eastern Arctic continental shelves

Accumulations of $N_2O$ up to ~25 nM have been reported across the productive and shallow (< 100 m) continental shelves of the western Arctic Ocean, including the Bering Sea, the Chukchi Sea

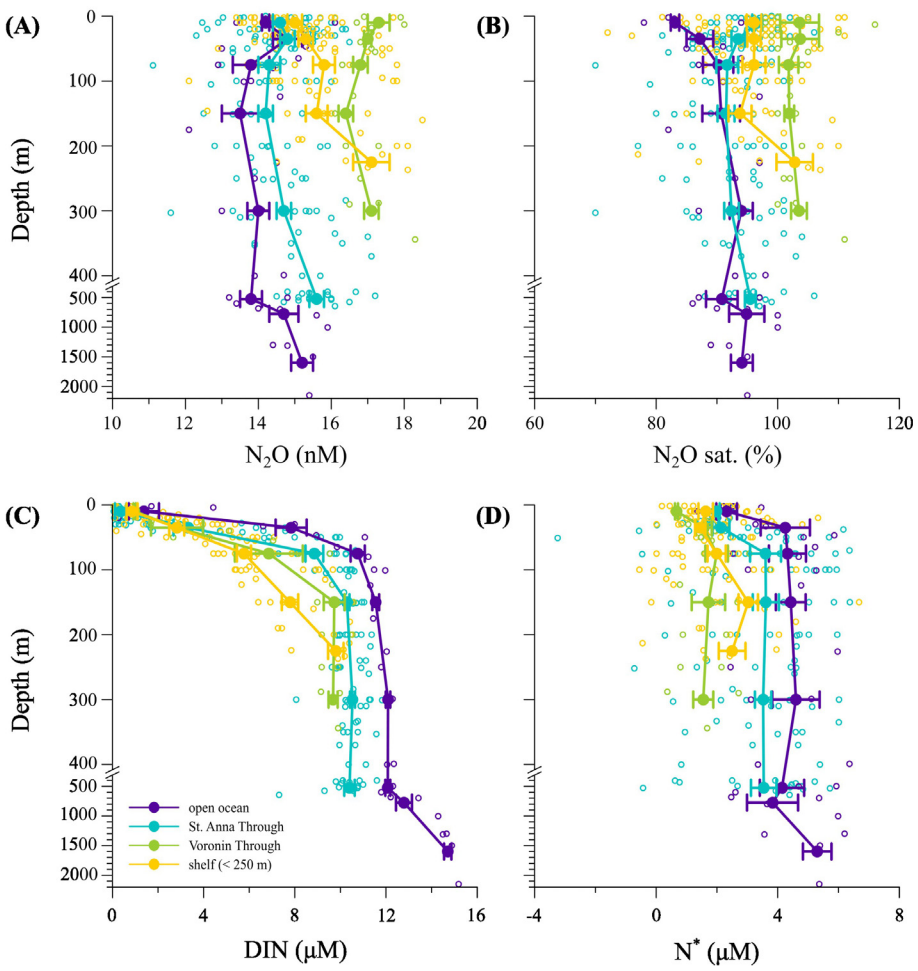


FIGURE 3
$N_2O$ **(A)**, $N_2O$ saturation **(B)**, DIN concentration **(C)** and N* concentration **(D)** vs depth. Empty circles represent the individual samples and the lines with filled circles represent the mean concentrations of each group of stations as defined in Figure 1, at specific depth ranges (0 m – 20 m; 20 m – 50 m; 50 m – 100 m; 100 m – 200 m; 200 m – 400 m; 400 m – 650 m; 650 m -1000 m; 1000 m – 2200 m). Each averaged point is calculated from at least three samples, except for the DIN surface point of the Voronin Trough (0 m – 20 m), that was calculated from two points due to lack of data. The error bars represent the standard error.

10.3389/fmars.2024.1497360

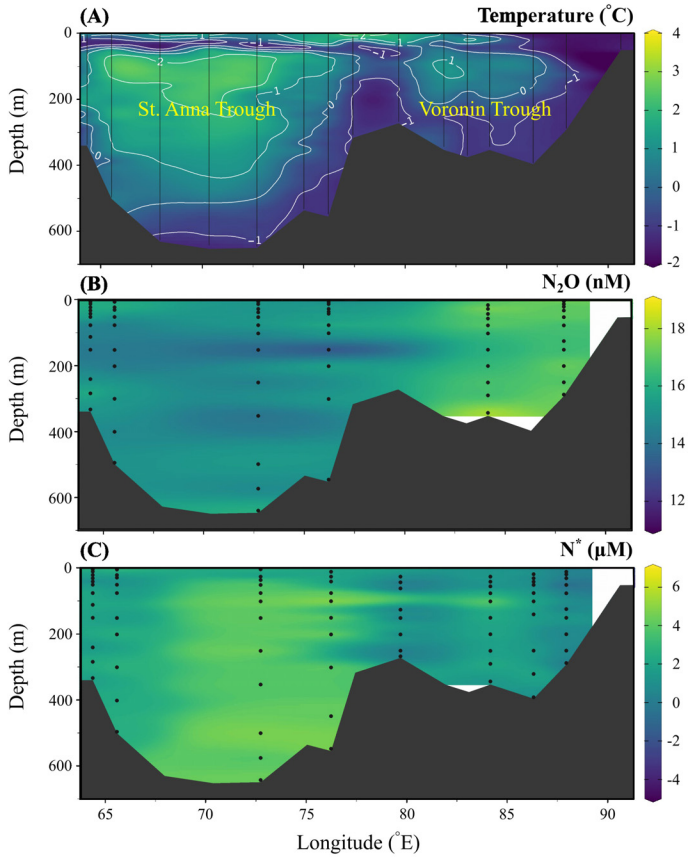


FIGURE 4
Depth sections of temperature **(A)**, $N_2O$ concentration **(B)** and N* **(C)** in the northern Kara Sea (transect shown with the black dashed line in Figure 1). Temperature data comes from CTD dataset (Hölemann et al., 2022).

and the Canadian Arctic Archipelago (Hirota et al., 2009; Fenwick et al., 2017; Manning et al., 2022). These shelves are partly influenced by nutrient-rich Pacific waters entering the Arctic Ocean through the Bering Strait (Grebmeier et al., 2006). The accumulation of $N_2O$ was mostly observed in shelf bottom waters, and showed a negative correlation with N*, suggesting that benthic denitrification or benthic coupled nitrification-denitrification processes were likely the sources of $N_2O$ (Hirota et al., 2009; Fenwick et al., 2017; Toyoda et al., 2021). However, there are also findings that indicated a positive correlation between $\Delta N_2O$ and AOU (Toyoda et al., 2021), suggesting that remineralization followed by nitrification, either in the reactive sedimentary layer or in the water column, may also contribute to the observed $N_2O$ accumulation (Nevison et al., 2003). Despite ongoing discussion about the precise mechanism accounting for the accumulation of $N_2O$, it is likely that this feature resulted from the enhanced productivity on continental shelves. Enhanced productivity is usually attributed to high nutrient availability at

TABLE 1 Short-term and monthly $N_2O$ air-sea fluxes computed from sea surface values.

| Region | Area ($km^2$) | $N_2O$ fluxes | | | | |
|---|---|---|---|---|---|---|
| | | $N_2O$ surface saturation range (%) | Flux range (µmol $N_2O$ $m^{-2}$ $d^{-1}$) | Mean ± sd short-term flux (µmol $N_2O$ $m^{-2}$ $d^{-1}$) | Median [1st Q, 3d Q] short-term flux (µmol $N_2O$ $m^{-2}$ $d^{-1}$) | 30-day flux (Gg N $month^{-1}$) |
| Northern Kara Sea (N = 27) | n.d. | [82, 111] | [-4.0, 1.8] | -0.6 ± 1.0 | -0.8 [-1.0, 0.0] | n.a. |
| Off-shelf (N = 2) | n.d. | [82, 84] | [-4.0, -1.8] | -2.9 ± 1.5 | n.a. | n.a. |
| Ice free northern Kara Sea (N = 19) | 209 308 | [90, 111] | [-2.4, 1.8] | -0.5 ± 0.9 | -0.8 [-0.9, 0.0] | -0.1 |

Positive values represent a flux from the sea to the air (source) and negative values a flux from the air to the sea (sink). The median surface saturation values are reported with the surface saturation range. The mean $N_2O$ flux values are reported with the standard deviation, and the median values with the first and third quartiles. Abbreviations n.a. and n.d. stand for not applicable and not determined, respectively.

the surface, due to enhanced upwelling and mixing, and proximity to terrestrial nutrient sources (Pabi et al., 2008; Tremblay et al., 2015; Terhaar et al., 2021). Elevated productivity leads, in turn, to elevated carbon export, abundant benthic carbon supply, and, therefore, enhanced benthic remineralization (Grebmeier et al., 2006). As a result, the water column and benthic biogeochemical cycling - including benthic denitrification and nitrification - are particularly linked and intensified on the continental shelves (Grebmeier et al., 2006; Chang and Devol, 2009; Granger et al., 2011). The $N_2O$-enriched shelf bottom waters of the western Arctic shelves, are then transported into the central basin, resulting in a persistent peak in $N_2O$ concentrations in the subsurface waters (Zhang et al., 2015; Fenwick et al., 2017; Heo et al., 2021; Toyoda et al., 2021; Manning et al., 2022).

Despite being influenced by nutrient-poor Atlantic waters, marginal seas in the eastern Arctic Ocean are characterized by primary productivity similar to the marginal seas in the western Arctic Ocean (Arrigo and van Dijken, 2011). High primary productivity may be attributed to a higher terrigenous nutrient supply via rivers and coastal erosion (Opsahl et al., 1999; Frey et al., 2007; Terhaar et al., 2021). Strong benthic-pelagic biogeochemical couplings have indeed been documented in the region, with evidence of benthic denitrification and benthic coupled nitrification-denitrification (Anderson et al., 2011; Fripiat et al., 2018; Sun et al., 2021). Accordingly, an increase in $N_2O$ concentrations in shelf bottom waters can be expected. This is supported by our observations, where an accumulation of $N_2O$ up to approximately 18 nM was reported in the Kara Sea. This accumulation was more important for shallower areas (Figure 3A) and exhibited a negative correlation with $N^*$ when considering the average depth profiles (p-value < 0.01 and $R^2$ = 33.4%; Figure 5A). No significant relationship (p-value ≥ 0.1) was found between $N_2O$ and DIN or between $\Delta N_2O$ and AOU (Figures 5B, C), suggesting that nitrification was not the main $N_2O$ production pathway. Benthic denitrification and/or benthic coupled nitrification-denitrification appear therefore to be the primary sources of $N_2O$ in shelf bottom waters throughout the Arctic Ocean.

The expression of the benthic-pelagic couplings on biogeochemical properties, including $N_2O$ concentration, of shelf bottom waters was likely correlated with the time that these waters spent over the continental shelves. Water residence times in the eastern Arctic continental shelves were estimated to range

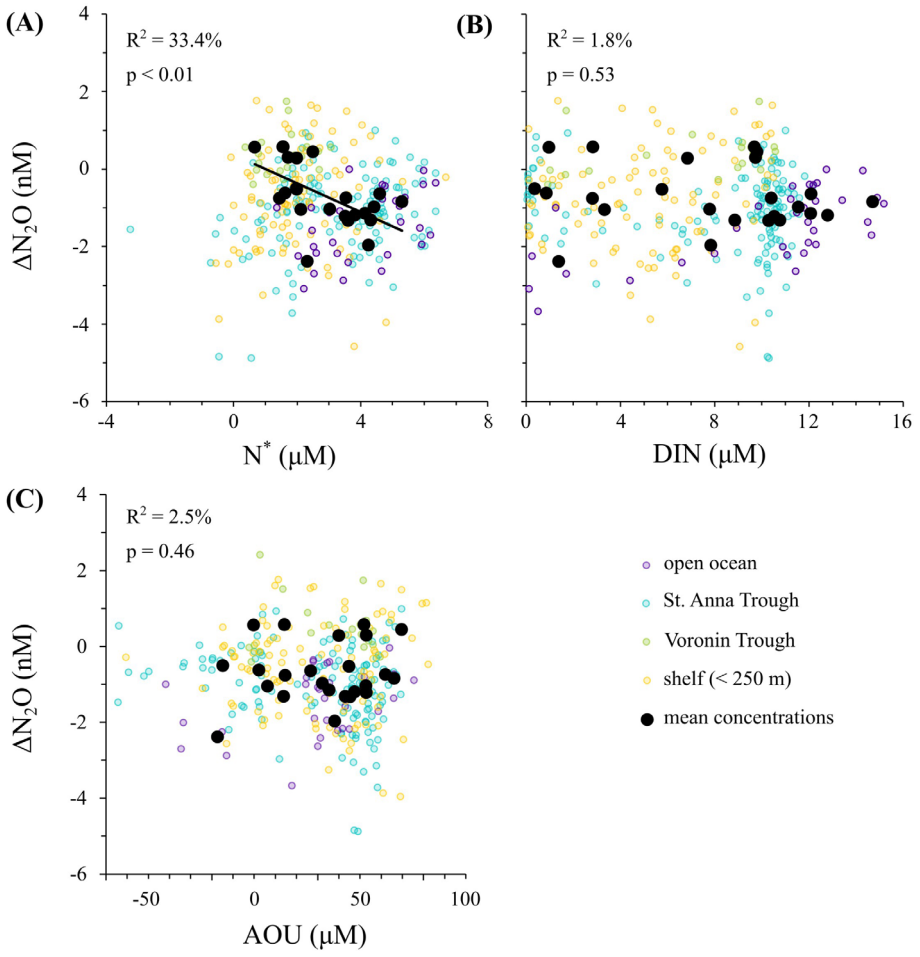


FIGURE 5
$N_2O$ versus N* **(A)** and DIN **(B)**, and $\Delta N_2O$ versus AOU **(C)**. Small circles represent individual samples, and the big filled black circles represent the mean concentrations of the samples, as described in Figure 2. Regression lines are shown where there is significant statistical correlation between the mean concentrations.

approximately between 1.5 years up to 5 years (Schlosser et al., 1994; Liu et al., 2019). The quasi-cyclonic circulation in the Kara Sea implies that shelf bottom waters in the Voronin Trough were exposed to the active sedimentary layer for the longest time (Figures 1 and 2), leading to higher concentrations of $N_2O$, lower concentrations of DIN and a more pronounced deficit in fixed N (denoted as lower N*; Figures 3A, C, D, 4B, C).

We estimated the required time to generate the observed increase in $N_2O$ concentration from the open ocean to the Voronin Trough (i.e., 2.0 ± 1.0 nM). By considering the average sediment-water $N_2O$ flux of 110 ± 116 nmol $m^{-2}$ $d^{-1}$, derived from sediment-core incubations in the Kara, Laptev, and East Siberian Seas (Wild et al., 2023), we estimated this time to be 10 ± 16 years for a water column of 200 m. Large uncertainties in the sedimentary flux preclude a more thorough analysis, although they fall within the range given by the residence time of the waters on eastern Arctic continental shelves. It is interesting to note that shorter residence times of shelf bottom waters were observed over the western Arctic shelves (0.1 - 2.3 years in Liu et al., 2019). Therefore, to replicate the $N_2O$ buildup observed in the shelf bottom waters of the western Arctic shelves, a higher $N_2O$ sedimentary flux would be required.

The $N_2O$ distribution in the water column over the shelves diverged from the results reported by Wild et al. (2023), which, to the best of our knowledge, is the sole study documenting $N_2O$ concentrations across the continental shelves of the eastern Arctic Ocean. This study encompasses the South Kara Sea near river mouths, the Laptev Sea, and the East Siberian Sea. Unlike our observations, the majority of their stations do not show an accumulation of $N_2O$ in shelf bottom waters. This divergence from our data and from previous findings in the western Arctic Ocean (Hirota et al., 2009; Fenwick et al., 2017; Manning et al., 2022) led Wild et al. (2023) to attribute this disparity to the intricate dynamics of $N_2O$. These dynamics likely involved production and consumption processes occurring within the water column, sediments, and particle microenvironments (Farías et al., 2013; Rees et al., 2016; Bianchi et al., 2018). The complexity of $N_2O$ dynamics warrants further investigation. Overall, our dataset suggests that $N_2O$ accumulation in the Arctic predominantly occurs in bottom shelf waters close to the reactive sedimentary layer, where benthic denitrification and coupled nitrification-denitrification takes place. However, the heterogeneity in our data (including some profiles showing decreasing trends with depth over the shelves) implies that $N_2O$ dynamics are more intricate than this conceptual view suggests, in agreement with Wild et al. (2023). Additional research, particularly process-based studies, is needed to fully comprehend these processes.

## 4.2 $N_2O$ undersaturation in intermediate and deep waters

The intermediate and deep waters of the open ocean and St. Anna Trough are undersaturated (Figure 3B). The undersaturation in intermediate and deep waters of the central Arctic Ocean has previously been reported in the literature (Zhang et al., 2015; Zhan et al., 2016; Fenwick et al., 2017; Manning et al., 2022). This undersaturation is attributed to the poor ventilation rates of the deep Arctic Ocean (Heo et al., 2021; Toyoda et al., 2021). This implies that these water masses were exposed to the atmosphere when atmospheric $N_2O$ concentrations were significantly lower than today (Schilt et al., 2014). The open ocean supplies mainly the St. Anna Trough, through FSBW (Figure 1), which is characterized by warmer intermediate water masses (i.e., temperatures > 0°C) as depicted in Figure 4A, leading to a similar undersaturation observed between the former and the latter (Figure 3B).

## 4.3 $N_2O$ saturation in the surface waters

In summer, surface waters over the Kara Sea shelves were on average near equilibrium or slightly undersaturated with respect to the atmosphere and might function as a minor sink (Figures 6, 7). As the equilibrium is controlled by solubility that is as function of the temperature, we observed a significant (p-value < 0.001 and $R^2$ = 33.5%) negative correlation between $N_2O$ concentrations and temperature in the mixed surface layer (Figure 8). On a broader scale, Zhan et al. (2017) observed a similar pattern. They reported a latitudinal gradient in $N_2O$ concentrations in surface waters, aligned with the latitudinal solubility gradient resulting from the change in sea surface temperature. Specifically, $N_2O$ concentrations were lowest in the warmer tropical and subtropical waters, while the highest concentrations were found in colder polar waters (Zhan et al., 2017).

Globally, $N_2O$ saturation (Equation 1) in the ocean is either close to equilibrium or slightly oversaturated for surface waters (Nevison et al., 2003; Zhan et al., 2017; Yang et al., 2020), resulting in a net source to the atmosphere (Tian et al., 2020, 2024; Yang et al., 2020). However, the Arctic Ocean exhibits a significant scatter in saturation levels compared to other areas (Zhan et al., 2017). The scattered distribution likely stems from the extensive and shallow continental shelves that span half of the Arctic Ocean (Harris et al., 2014; Zhan et al., 2017). These shelves host diverse biogeochemical processes, including primary production, organic matter decomposition, nitrogen cycling (i.e., nitrification and denitrification), and carbon sequestration, which are influenced by varying levels of vertical mixing and river discharge (Aagaard and Carmack, 1989; Opsahl et al., 1999; Terhaar et al., 2021). Furthermore, factors such as the presence of sea ice and generally low wind speeds prevent air-sea gas exchange (Butterworth and Miller, 2016; Rutgers van der Loeff et al., 2014; Zhan et al., 2017), yielding local minima and maxima in $N_2O$ saturation. In the Arctic Ocean, oversaturation values (reaching up to 157%) have been reported over the shallow continental shelves, while the central Arctic Ocean experiences saturation values either close to the equilibrium or undersaturated (Hirota et al., 2009; Zhang et al., 2015; Fenwick et al., 2017; Zhan et al., 2017; Manning et al., 2022; Wild et al., 2023). The occurrence of oversaturation over continental shelves is attributed to the substantial $N_2O$ production within the active sedimentary layer, which then diffuses into the overlying water column and hence, the atmosphere. These oversaturation are often reported close to marginal ice zones or sea ice covered areas, since sea ice inhibits air-sea gas exchange (Kitidis et al., 2010; Fenwick et al., 2017; Manning et al., 2022). Conversely, the undersaturation in the

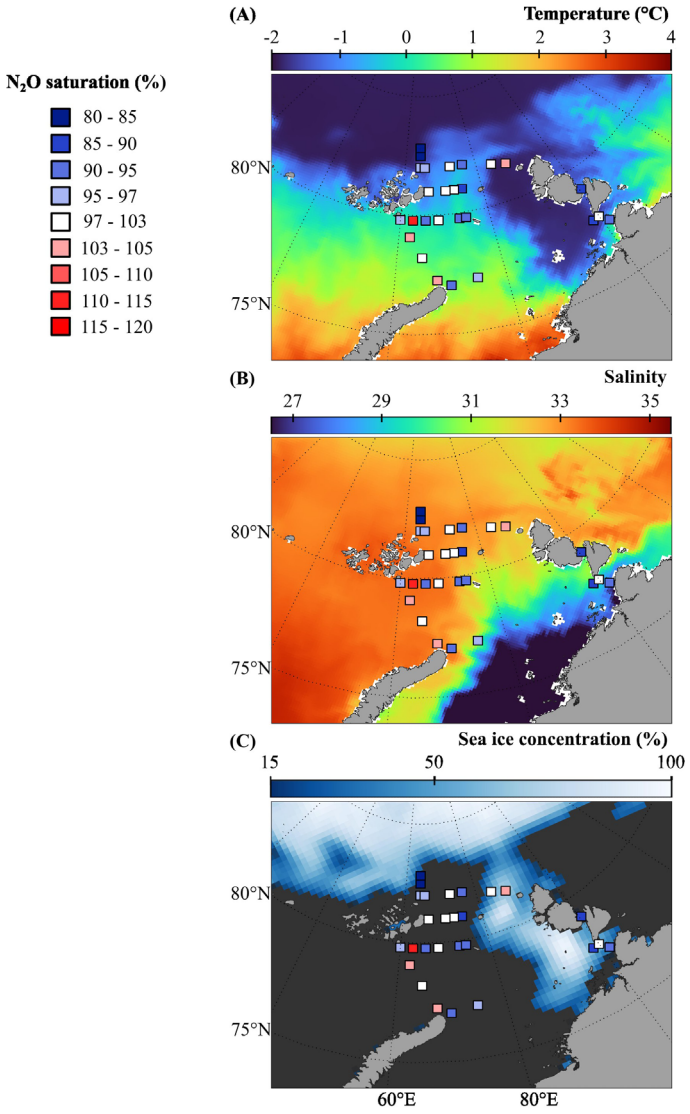


FIGURE 6
Distribution of $N_2O$ saturation in the sea surface waters (coloured squares). Background contours show sea surface temperature **(A)**, sea surface salinity **(B)**, and sea ice concentration **(C)** on August 21st, 2021. Ice-free ocean is represented in dark grey in panel **(C)**. Data is available on the Copernicus Marine Service for sea surface temperature and salinity (doi:10.48670/moi-00016), and sea ice concentration (doi: 10.48670/moi-00136).

central Arctic Ocean or the shelves is usually attributed to several factors, including: the dilution by sea-ice meltwater (i), rapid cooling of surface waters (ii), upwelling of undersaturated deep waters (iii), or microbiological $N_2O$ consumption (iv) (Kitidis et al., 2010; Randall et al., 2012; Verdugo et al., 2016; Zhan et al., 2016; Liu et al., 2022; Wild et al., 2023). Our study confirms this spatial heterogeneity in surface $N_2O$ saturation (Figure 6). Specifically, we observed 15 stations with undersaturated values (below 97%), 8 stations close to the equilibrium (i.e., between 97-103%) and 4 stations with oversaturated values (i.e., above 103%).

We observed significant undersaturation in $N_2O$, down to 80%, off the shelf at the two open ocean stations located North of 82°N (Figure 6). A lower degree of undersaturation was also observed South of the open ocean stations, at the northwestern stations of the Kara Sea, influenced by the inflow of surface waters from the FSBW (Figures 1, 6). Sea surface temperature at these stations was close to the freezing point (-1.6°C to – 1.4°C for the two open ocean stations; Figure 6A). This suggests that these waters were recently below sea ice, consistent with their proximity to the sea ice edge and ocean circulation (Figures 2, 6C). Our assumption attributes this undersaturation to water cooling coupled to limited air-sea exchange. The surface waters cool down as they enter the Arctic Ocean's sea ice zone through Fram Strait or during winter in the central Arctic Ocean, enhancing solubility resulting in undersaturation. The deficit cannot be offset due to restrained air-sea gas exchange inherent to sea ice cover (Rutger van der Loeff et al., 2014), along their transit to the Kara Sea. Furthermore, the possibility of vertical mixing with undersaturated deep waters may contribute to this surface water undersaturation, as observed by Zhan et al. (2016) in the Greenland Basin. However, contrary to

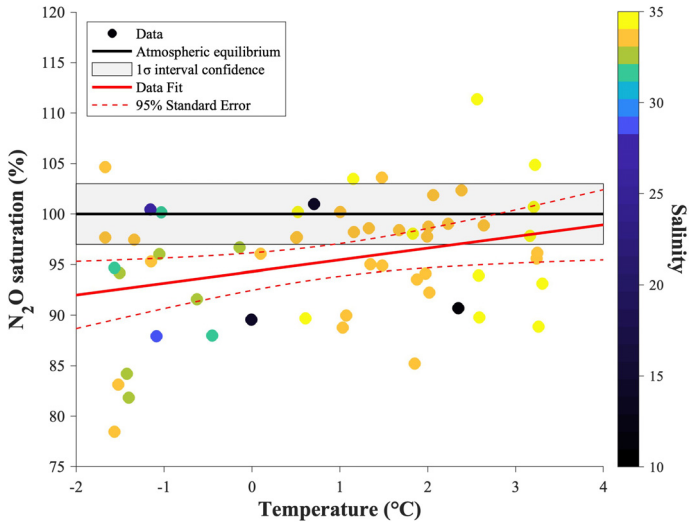


FIGURE 7
$N_2O$ saturations (%) in the mixed surface layer. The $N_2O$ saturation (y axis) is compared to the temperature (°C; x axis) and salinity (colorbar). The black line and grey shade represent the equilibrium state (at 100%) and saturation error (2σ), respectively. The solid and dashed red lines represent the fit of the data with the standard error, respectively. It is observed that most of the MSL is at equilibrium with the atmosphere with regard $N_2O$. The saturation deficit is the strongest for temperatures near the freezing point. The samples with a river signal are at equilibrium or undersaturated.

Zhan et al. (2016), we observe a decrease in saturation towards the surface, suggesting that additional processes are required to explain the observed undersaturation.

To test our hypothesis, we quantified the change in solubility caused by changes in temperature and salinity. The temperature effect was examined by cooling the water mass, while the salinity effect was induced by the melting of sea ice. Our analysis focused on a water mass near the equilibrium point ($N_2O$ saturation of 100%), and we prescribed an initial sea surface temperature, salinity and $N_2O$ concentration at 2°C, 34 and 14.5 nM, respectively. These conditions are representative of surface water in the Kara Sea in equilibrium with the atmosphere (Figure 7). We then calculated the amount of ice meltwater required to reach a salinity of 32, which resulted in a corresponding concentration of 13.7 nM when assuming a concentration of 2.1 nM in sea ice. We assume that sea ice concentration follows a conservative behavior, i.e., a linear relationship between $N_2O$ concentration and salinity. When considering only ice meltwater, the $N_2O$ saturation decreased from 100% to 93%, indicating a relatively weak impact from the dilution effect of ice meltwater and solubility effect of salinity. However, when solely considering the temperature effect (i.e., a cooling from 2°C to -1.8°C at a salinity of 34), the saturation

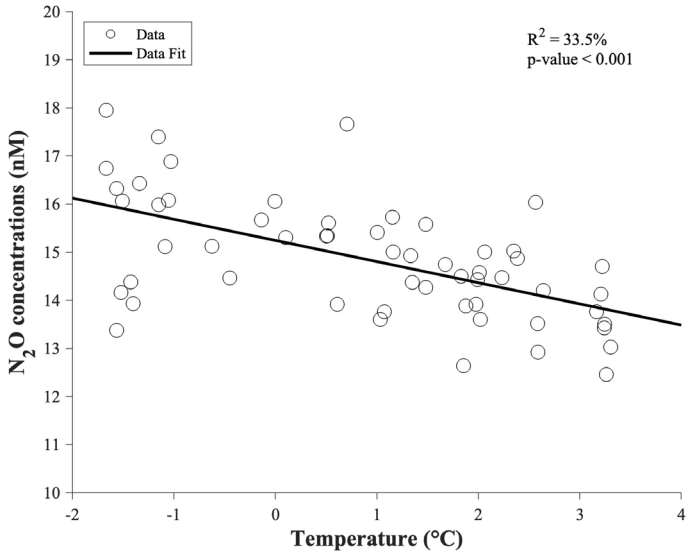


FIGURE 8
$N_2O$ concentrations in the mixed surface layer. The $N_2O$ concentration is compared to temperature. The regression line is shown in black.

dropped to 85%. By combining both effects (i.e., ice meltwater and water cooling), we were able to replicate the observed saturation of 80%. These suggest that the significant undersaturation observed at these stations are influenced by physical processes, with three quarters attributed to a cooling effect and one quarter to sea-ice meltwater. Considering the mixed layer depth of 12 m at these stations, an estimated 0.9 m of melted sea ice thickness per $m^2$ would be required to reach that salinity, which, while significant, remains possible (Karvonen et al., 2022).

The eastern coastal stations located at 100°E, exhibited elevated concentrations of $N_2O$, as the Voronin Trough (S. 2), but with lower saturation levels ranging from 90% to 101% (Figure 6). This area is under the influence of river discharge, characterized by its overall lower sea surface salinity (Figure 6B). Enhanced concentration in $N_2O$ can be due to $N_2O$ supply from the rivers but also due to enhanced pelagic – benthic coupling in shallow bathymetries and over the shelves. In addition, higher concentrations can be due to atmospheric $N_2O$ uptake, given that these waters are undersaturated in $N_2O$ relative to the atmosphere. Wild et al. (2023), who also found little relationship between $N_2O$ and salinity in the plume of the Ob and Yenisey rivers, suggested that the processes at play are more intricate that a simple $N_2O$ supply from the rivers. We attribute the saturation deficit to a salinity effect on solubility that outweighs enhanced $N_2O$ concentration. For instance, if we consider a water mass in equilibrium with the atmosphere representative of the northern Kara Sea as above (i.e., 14,5 nM with a temperature of 2°C and salinity of 34 for 100% saturation), a decrease in the salinity to 14.6, a change in temperature to 0°C, and a constant $N_2O$ concentration, as observed in the river discharge area, would lead to a significant change in saturation down to 82%. Consequently, the Ob and Yenisey rivers are not contributing to an enriched $N_2O$ signal that would serve as a source to the atmosphere but likely promote undersaturation and $N_2O$ uptake in summer.

Oversaturation was observed in four stations (stations 1, 10, 16 and 59 in Figure 6 and Supplementary Figure S1A), three are located on the western side of the Kara Sea, at the entrance of the Barents Sea, and one in the Voronin Trough. The common point between these stations is that they are all categorized as shelf stations, meaning that their water column is, on average, enriched in $N_2O$ (Figure 3). Oversaturation at the entrance of the Barents Sea may result from the mixing between $N_2O$-poor, warm and saline surface waters from the Barents Sea with $N_2O$-rich, cold and fresh surface waters in the Kara Sea. (S. 2A). Knowing that a change of 1°C in temperature induces a change of approximately 5% in $N_2O$ saturation while preserving the $N_2O$ concentration, these conditions would yield oversaturation, implying that this change in solubility is occurring faster than air-sea exchange. There is a semi-cyclonic circulation in the St. Anna Trough, where the warmer and oversaturated waters flow northward, and the colder and undersaturated waters flow southward (Figures 2 and 6A). This water circulation caused the stations in the central St. Anna Trough to reach equilibrium with the atmosphere while forming a latitudinal saturation gradient.

The oversaturation of the surface waters in the Voronin Trough likely results from the $N_2O$ production integrated over the continental shelf of the Kara Sea and exiting the Kara Sea via the Voronin Trough (Figures 1, 2). The presence of sea ice in this area (Figure 6S) prevents surface waters from reaching atmospheric equilibrium, inhibiting air-sea gas exchange (Rutgers van der Loeff et al., 2014). Fenwick et al. (2017) and Kitidis et al. (2010) observed a similar tendency of $N_2O$ build-up and oversaturation under sea ice covered areas in the Canadian Archipelago.

## 4.4 $N_2O$ sea-air fluxes

Our observations in the northern Kara Sea suggest that the area acts as a minor sink during summertime (Table 1). Mean $N_2O$ sea-air fluxes in this study (-0.6 µmol $N_2O$ $m^{-2}$ $d^{-1}$) are reasonably close to previous studies in the western shelves of the Arctic Ocean (Fenwick et al., 2017; Manning et al., 2022), ranging between -1 µmol $N_2O$ $m^{-2}$ $d^{-1}$ to 0 µmol $N_2O$ $m^{-2}$ $d^{-1}$. By contrast, the mean flux in this study is much lower than the mean value measured in the Kara Sea by Wild et al. (2023), who measured positive fluxes up to 58.1 µmol $N_2O$ $m^{-2}$ $d^{-1}$. An explanation for our lower $N_2O$ fluxes observed can be attributed to the comparatively narrower range of $N_2O$ saturation observed in our study, as opposed to Wild et al. (2023), who observed a larger spatial variability in surface waters of the eastern Arctic shelves. We denoted a stronger sink for the off-shelf stations (Table 1), which is related to the enhanced $N_2O$ undersaturation compared to on-shelf stations. As explained in section 4.3, this strong undersaturation at these stations results from a combination of increased solubility that is driven by cooling and sea ice melting and the presence of sea ice that inhibited air-sea exchange prior to being transported into the area.

Based on the average sea-air fluxes and considering solely the ice-free zone, we computed the monthly average emission of $N_2O$ during summertime for the northern Kara Sea to be -0.1 Gg N $month^{-1}$ (Table 1). As the area is undergoing substantial changes in sea ice melting and retreat during summer (S3) and the river discharge can drastically change with the season (Holmes et al., 2012), we did not consider our dataset to be representative of an annual average, but it underlines that the Kara Sea can act as $N_2O$ sink for the atmosphere. This calls for further fall to spring measurements in the continental shelf area.

# 5 Conclusion

Our study provides an analysis of $N_2O$ dynamics across the eastern Arctic shelves, in the Kara Sea during summertime. Despite the observed heterogeneity between $N_2O$ vertical profiles, an overall pattern indicates accumulation of $N_2O$ in the bottom waters of the Kara Sea shelves. Similar $N_2O$ enrichment was observed for the Voronin Trough, that receives water from the shallow shelves on their transit to the central Arctic Ocean. In contrast, low $N_2O$ accumulation was observed in the intermediate and deep waters of

the open ocean and St. Anna Trough areas. $N_2O$-enrichment correlated with N* deficit but showed no significant relationship with DIN nor AOU. Accumulation of $N_2O$ in shelf bottom waters is likely driven by benthic denitrification and/or coupled benthic nitrification-denitrification processes, and appears to be modulated by residence times of shelf bottom waters in contact with the reactive sedimentary layer.

In surface waters, $N_2O$ saturation was in average close to equilibrium with the atmosphere. Changes in solubility that are driven by temperature appeared as the main controlling factor for surface $N_2O$ concentration and saturation. Some spatial heterogeneity in surface saturation values resulted from the effects of freshwater discharge from the rivers and the presence of sea ice. River discharge would promote undersaturation, while sea ice would inhibit air-sea exchange, promoting either undersaturation or $N_2O$ build-up underneath or nearby. Air-sea exchange estimates determined that the Kara Sea acts as a minor sink during summertime.

These findings, and especially the spatial variability, highlight the complex interplay of physical and biogeochemical processes governing $N_2O$ dynamics in the Arctic Ocean and underscore the necessity for further process-based studies to enhance our understanding of these mechanisms. The climate-driven shift the Arctic Ocean is undergoing may potentially alter the nitrogen cycle and $N_2O$ dynamics in response to changing Arctic environments.

## Data availability statement

The $N_2O$ dataset for this study can be found on the Arctic Century repository on PANGEA doi: 10.1594/PANGAEA.973143. The nutrient dataset for this study can be found on the Arctic Century repository on PANGEA doi: 10.1594/PANGAEA.973439. The wind speed dataset for this study can be found on the Arctic Century repository on PANGEA doi: 10.3929/ethz-b-000693692. Absolute geostrophic velocity data is available through the Copernicus Climate Service https://climate.copernicus.eu/, product name "Global Ocean Gridded L 4 Sea Surface Heights And Derived Variables Reprocessed Copernicus Climate Service" (product ID: SEALEVEL_GLO_PHY_CLIMATE_L4_MY_008_057; doi:10.48670/moi-00145).

## Author contributions

SM: Data curation, Formal analysis, Software, Writing – original draft, Writing – review & editing. FF: Writing – original draft, Writing – review & editing, Supervision. SJ: Writing – review & editing. LP: Software, Writing – review & editing. JH: Data curation, Writing – review & editing. AM-G: Writing – review & editing. BD: Supervision, Writing – original draft, Writing – review & editing.

## Funding

The author(s) declare that financial support was received for the research, authorship, and/or publication of this article. This work was supported by the F.R.S-FNRS (grants J.0051.20 and J.0060.22). BD has received funding from GreenFeedBack (Greenhouse gas fluxes and earth system feedback) funded by the European Union's HORIZON research and innovation program under grant agreement No 101056921. Views and opinions expressed are however those of the authors only and do not necessarily reflect those of the European Union or CINEA. Neither the European Union nor the granting authority can be held responsible for them. SM & BD are FRIA PhD student and Research Associate, respectively, at the F.R.S.-FNRS.

## Acknowledgments

We thank the chief scientist Heidi Kassens, and the Master and the crew of the RV Akademik Tryoshnikov for their support in sample collection. Arctic Century expedition funded by the Swiss Polar Foundation, a joint initiative led by the Swiss Polar Institute, the Antarctic and Arctic Research Institute and GEOMAR Helmholtz Centre for Ocean Research Kiel (GEOMAR) under the auspices of the research project The Changing Arctic Transpolar System (CATS). We also thank Iris Thurnherr for sharing the wind speed data with us.

## Conflict of interest

The authors declare that the research was conducted in the absence of any commercial or financial relationships that could be construed as a potential conflict of interest.

## Publisher's note



## Supplementary material

The Supplementary Material for this article can be found online at: https://www.frontiersin.org/articles/10.3389/fmars.2024.1497360/full#supplementary-material

# References


Aagaard, K., and Carmack, E. C. (1989). The role of sea ice and other fresh water in the Arctic circulation. *J. Geophysical Research: Oceans* 94, 14485–14498. doi: 10.1029/JC094iC10p14485

Anderson, L. G., Björk, G., Jutterström, S., Pipko, I., Shakhova, N., Semiletov, I., et al. (2011). East Siberian Sea, an Arctic region of very high biogeochemical activity. *Biogeosciences* 8, 1745–1754. doi: 10.5194/bg-8-1745-2011

Arctic Ocean Physics Analysis and Forecast. Available online at: https://data.marine.copernicus.eu/product/ARCTIC_ANALYSISFORECAST_PHY_002_001/description (Accessed July 5, 2024).

Arrigo, K. R., and van Dijken, G. L. (2011). Secular trends in Arctic Ocean net primary production. *J. Geophysical Research: Oceans* 116, C09011. doi: 10.1029/2011JC007151

*Global ocean gridded L 4 sea surface heights and derived variables reprocessed copernicus climate service*. In: *Copernicus marine service*. Available online at: https://data.marine.copernicus.eu/product/SEALEVEL_GLO_PHY_CLIMATE_L4_MY_008_057/description (Accessed May 31, 2024).

*Global ocean sea ice concentration time series REPROCESSED (OSI-SAF)*. Available online at: https://data.marine.copernicus.eu/product/SEAICE_GLO_SEAICE_L4_REP_OBSERVATIONS_011_009/description (Accessed May 31, 2024).

Bange, H. W.. (2008). "Chapter 2 - Gaseous nitrogen compounds (NO, N2O, N2, NH3) in the ocean," in *Nitrogen in the marine environment (Second edition)* Ed. D. G. Capone, D. A. Bronk, M. R. Mulholland and E. J. Carpenter (Academic Press, San Diego), 51–94. doi: 10.1016/B978-0-12-372522-6.00002-5

Bianchi, D., Dunne, J. P., Sarmiento, J. L., and Galbraith, E. D. (2012). Data-based estimates of suboxia, denitrification, and N2O production in the ocean and their sensitivities to dissolved O2. *Global Biogeochemical Cycles* 26, GB2009. doi: 10.1029/2011GB004209

Bianchi, D., Weber, T. S., Kiko, R., and Deutsch, C. (2018). Global niche of marine anaerobic metabolisms expanded by particle microenvironments. *Nat. Geosci.* 11, 263–268. doi: 10.1038/s41561-018-0081-0

Bothe, H., Jost, G., Schloter, M., Ward, B. B., and Witzel, K. (2000). Molecular analysis of ammonia oxidation and denitrification in natural environments. *FEMS Microbiol. Rev.* 24, 673–690. doi: 10.1111/j.1574-6976.2000.tb00566.x

Brandes, J. A., and Devol, A. H. (2002). A global marine-fixed nitrogen isotopic budget: Implications for Holocene nitrogen cycling. *Global Biogeochemical Cycles* 16, 67-1-67–14. doi: 10.1029/2001GB001856

Butterworth, B. J., and Miller, S. D. (2016). Air-sea exchange of carbon dioxide in the Southern Ocean and Antarctic marginal ice zone. *Geophysical Res. Lett.* 43, 7223–7230. doi: 10.1002/2016GL069581

Chang, B. X., and Devol, A. H. (2009). Seasonal and spatial patterns of sedimentary denitrification rates in the Chukchi sea. *Deep Sea Res. Part II: Topical Stud. Oceanography* 56, 1339–1350. doi: 10.1016/j.dsr2.2008.10.024

Cohen, Y., and Gordon, L. I. (1979). Nitrous oxide production in the Ocean. *J. Geophysical Research: Oceans* 84, 347–353. doi: 10.1029/JC084iC01p00347

de Boyer Montégut, C., Madec, G., Fischer, A. S., Lazar, A., and Ludicone, D. (2004). Mixed layer depth over the global ocean: An examination of profile data and a profile-based climatology. *J. Geophysical Research: Oceans* 109, C12003. doi: 10.1029/2004JC002378

Devol, A. H., Codispoti, L. A., and Christensen, J. P. (1997). Summer and winter denitrification rates in western Arctic shelf sediments. *Continental Shelf Res.* 17, 1029–1050. doi: 10.1016/S0278-4343(97)00003-4

Farías, L., Faúndez, J., Fernández, C., Cornejo, M., Sanhueza, S., and Carrasco, C. (2013). Biological N2O fixation in the Eastern South Pacific Ocean and marine cyanobacterial cultures. *PloS One* 8, e63956. doi: 10.1371/journal.pone.0063956

Fenwick, L., Capelle, D., Damm, E., Zimmermann, S., Williams, W. J., Vagle, S., et al (2017). Methane and nitrous oxide distributions across the North American Arctic Ocean during summe. *J. Geophysical Research: Oceans* 122, 390–412. doi: 10.1002/2016JC012493

Frey, K. E., McClelland, J. W., Holmes, R. M., and Smith, L. C. (2007). Impacts of climate warming and permafrost thaw on the riverine transport of nitrogen and phosphorus to the Kara Sea. *J. Geophysical Research: Biogeosciences* 112, G04S58. doi: 10.1029/2006JG000369

Fripiat, F., Declercq, M., Sapart, C. J., Anderson, L. G., Bruechert, V., Deman, F., et al. (2018). Influence of the bordering shelves on nutrient distribution in the Arctic halocline inferred from water column nitrate isotopes. *Limnology Oceanography* 63, 2154–2170. doi: 10.1002/lno.10930

Gangnus, I., Makhotin, M., Cherniavskaia, E., Hölemann, J. A., Kusse-Tiuz, N., Lavinen, N., et al. (2022). Nutrients, oxygen, total alkalinity, pH, and physical oceanography measured on water bottle samples during Akademik Tryoshnikov cruise Arctic Century 2021 Expedition (AT21), Arctic Ocean. *PANGAEA*. doi: 10.1594/PANGAEA.947808

Granger, J., Prokopenko, M. G., Sigman, D. M., Mordy, C. W., Morse, Z. M., Morales, L. V., et al. (2011). Coupled nitrification-denitrification in sediment of the eastern Bering Sea shelf leads to 15N enrichment of fixed N in shelf waters. *J. Geophysical Research: Oceans* 116, C11006. doi: 10.1029/2010JC006751

Grebmeier, J. M., Cooper, L. W., Feder, H. M., Sirenko, B. I., et al. (2006). Ecosystem dynamics of the pacific-influenced northern bering and chukchi seas in the amerasian arctic. *Prog. Oceanography* 71, 331–361. doi: 10.1016/j.pocean.2006.10.001

Gruber, N., and Sarmiento, J. L. (1997). Global patterns of marine nitrogen fixation and denitrification. *Global Biogeochemical Cycles* 11, 235–266. doi: 10.1029/97GB00077

Harris, P. T., Macmillan-Lawler, M., Rupp, J., and Baker, E. K. (2014). Geomorphology of the oceans. *Mar. Geology* 352, 4–24. doi: 10.1016/j.margeo.2014.01.011

Heo, J.-M., Kim, S.-S., Kang, S.-H., Yang, E. J., Park, K.-T., Jung, J., et al. (2021). N2O dynamics in the western Arctic Ocean during the summer of 2017. *Sci. Rep.* 11, 12589. doi: 10.1038/s41598-021-92009-1

Hirota, A., Ijiri, A., Komatsu, D. D., Ohkubo, S. B., Nakagawa, F., and Tsunogai, U. (2009). Enrichment of nitrous oxide in the water columns in the area of the Bering and Chukchi Seas. *Mar. Chem.* 116, 47–53. doi: 10.1016/j.marchem.2009.09.001

Ho, D. T., Law, C. S., Smith, M. J., Schlosser, P., Harvey, M., Hill, P., et al. (2006). Measurements of air-sea gas exchange at high wind speeds in the Southern Ocean: Implications for global parameterizations. *Geophysical Res. Lett.* 33, L16611. doi: 10.1029/2006GL026817

Hölemann, J. A., Kusse-Tiuz, N., Ruiz-Castillo, E., Malinovskiy, S., Merkulov, V., Burkhardt, M., et al. (2022). Physical oceanography measured with Underway-CTD (UCTD) during Akademik Tryoshnikov cruise Arctic Century 2021 Expedition (AT21), Arctic Ocean. *PANGAEA*. doi: 10.1594/PANGAEA.947810

Holmes, R. M., McClelland, J. W., Peterson, B. J., Tank, S. E., Bulygina, E., Eglinton, T. I., et al. (2012). Seasonal and annual fluxes of nutrients and organic matter from large rivers to the arctic ocean and surrounding seas. *Estuaries Coasts* 35, 369–382. doi: 10.1007/s12237-011-9386-6

Hsu, S. A., Meindl, E. A., and Gilhousen, D. B. (1994). Determining the Power-Law Wind-Profile Exponent under Near-Neutral Stability Conditions at Sea. *J. Appl. Meteorology Climatology* 33, 757–765. doi: 10.1175/1520-0450(1994)033<0757:DTPLWP>2.0.CO;2

Hydes, D. J., Aoyama, M., Aminot, A., Bakker, K., Becker, S., Coverly, S., et al. (2010). Determination of dissolved nutrients (N, P, SI) in seawater with high precision and inter-comparability using gas-segmented continuous flow analysers. doi: 10.25607/OBP-15

IPCC (2023). "*Climate change 2023: synthesis report. Contribution of working groups I, II and III to the sixth assessment report of the intergovernmental panel on climate change [Core writing team, H. Lee and J. Romero (eds.)].*," (IPCC, Geneva, Switzerland), p. 184. doi: 10.59327/IPCC/AR6-9789291691647

Janout, M. A., Hölemann, J., Laukert, G., Smirnov, A., Krumpen, T., Bauch, D., et al. (2020). On the variability of stratification in the freshwater-influenced laptev sea region. *Front. Mar. Sci.* 7. doi: 10.3389/fmars.2020.543489

Karvonen, J., Rinne, E., Sallila, H., Uotila, P., and Mäkynen, M. (2022). Kara and Barents sea ice thickness estimation based on CryoSat-2 radar altimeter and Sentinel-1 dual-polarized synthetic aperture radar. *Cryosphere* 16, 1821–1844. doi: 10.5194/tc-16-1821-2022

Kitidis, V., Upstill-Goddard, R. C., and Anderson, L. G. (2010). Methane and nitrous oxide in surface water along the North-West Passage, Arctic Ocean. *Mar. Chem.* 121, 80–86. doi: 10.1016/j.marchem.2010.03.006

Liu, X., Dunne, J. P., Stock, C. A., Harrison, M. J., Adcroft, A., and Resplandy, L. (2019). Simulating water residence time in the coastal ocean: A global perspective. *Geophysical Res. Lett.* 46, 13910–13919. doi: 10.1029/2019GL085097

Liu, J., Zhan, L., Wang, Q., Wu, M., Ye, W., Zhang, J., et al. (2022). Distribution and driving mechanism of N2O in sea ice and its underlying seawater during arctic melt season. *Water* 14, 145. doi: 10.3390/w14020145

Liu, J., Chen, L., Ling, M., Zhuang, Y., Zhang, J., Ye, W., et al. (2024). Potential contributions of ammonia-oxidizing microorganisms to the distributions of nitrous oxide in the northern bering sea. *J. Geophysical Research: Oceans* 129, e2023JC020677. doi: 10.1029/2023JC020677

Makkaveev, P. N., Melnikova, Z. G., Polukhin, A. A., Stepanova, S. V., Khlebopashev, P. V., and Chultsova, A. L. (2015). Hydrochemical characteristics of the waters in the western part of the Kara Sea. *Oceanology* 55, 485–496. doi: 10.1134/S0001437015040116

Manning, C. C. M., Zheng, Z., Fenwick, L., McCulloch, R. D., Damm, E., Izett, R. W., et al. (2022). Interannual variability in methane and nitrous oxide concentrations and sea-air fluxes across the north american arctic ocean (2015-2019). *Global Biogeochemical Cycles* 36, e2021GB007185. doi: 10.1029/2021GB007185

McClelland, J. W., Holmes, R. M., Peterson, B. J., Raymond, P. A., Striegl, R. G., Zhulidov, A. V., et al. (2016). Particulate organic carbon and nitrogen export from major Arctic rivers. *Global Biogeochemical Cycles* 30, 629–643. doi: 10.1002/2015GB005351

McTigue, N. D., Gardner, W. S., Dunton, K. H., and Hardison, A. K. (2016). Biotic and abiotic controls on co-occurring nitrogen cycling processes in shallow Arctic shelf sediments. *Nat. Commun.* 7, 13145. doi: 10.1038/ncomms13145

Muller, S., Jaccard, S. L., Hölemann, J. A., Fripiat, F., Martínez-García, A., Makhotin, M., et al. (2024). N2O concentrations measured on water bottle samples during

Akademik Tryoshnikov cruise Arctic Century 2021 Expedition (AT21), Arctic Ocean. *PANGAEA*. doi: 10.1594/PANGAEA.973143

Muller, S., Fripiat, F., Schmitt, M., Jaccard, S. L., Hölemann, J. A., Delille, B., et al. (2024). Nutrients concentrations measured on water bottle samples during Akademik Tryoshnikov cruise Arctic Century 2021 Expedition (AT21), Arctic Ocean [dataset]. *PANGAEA*. doi: 10.1594/PANGAEA.973439

Nevison, C., Butler, J. H., and Elkins, J. W. (2003). Global distribution of N2O and the ΔN2O-AOU yield in the subsurface ocean. *Global Biogeochemical Cycles* 17, 1119. doi: 10.1029/2003GB002068

Opsahl, S., Benner, R., and Amon, R. M. W. (1999). Major flux of terrigenous dissolved organic matter through the Arctic Ocean. *Limnology Oceanography* 44, 2017–2023. doi: 10.4319/lo.1999.44.8.2017

Pabi, S., van Dijken, G. L., and Arrigo, K. R. (2008). rimary production in the arctic ocean 1998-2006. *J. Geophysical Research: Oceans* 113, C08005. doi: 10.1029/2007JC004578

Randall, K., Scarratt, M., Levasseur, M., Michaud, S., Xie, H., and Gosselin, M. (2012). First measurements of nitrous oxide in Arctic sea ice. *J. Geophysical Research: Oceans* 117, C00G15. doi: 10.1029/2011JC007340

Ravishankara, A. R., Daniel, J. S., and Portmann, R. W. (2009). Nitrous oxide (N2O): the dominant ozone-depleting substance emitted in the 21st century. *Science* 326, 123–125. doi: 10.1126/science.1176985

Rees, A. P., Brown, I. J., Jayakumar, A., and Ward, B. B. (2016). The inhibition of N2O production by ocean acidification in cold temperate and polar waters. *Deep Sea Res. Part II: Topical Stud. Oceanography* 127, 93–101. doi: 10.1016/j.dsr2.2015.12.006

Rowe, G. T., CliQord, C. H., Smith, K. L., and Hamilton, P. L. (1975). Benthic nutrient regeneration and its coupling to primary productivity in coastal waters. *Nature* 255, 215–217. doi: 10.1038/255215a0

Rutgers van der Loeff, M. M., Cassar, N., Nicolaus, M., Rabe, B., and Stimac, I. (2014). The influence of sea ice cover on air-sea gas exchange estimated with radon-222 profiles. *J. Geophysical Research: Oceans* 119, 2735–2751. doi: 10.1002/2013JC009321

Schilt, A., Brook, E. J., Bauska, T. K., Baggenstos, D., Fischer, H., Joos, F., et al. (2014). Isotopic constraints on marine and terrestrial N2O emissions during the last deglaciation. *Nature* 516, 234–237. doi: 10.1038/nature13971

Schlosser, P., Bauch, D., Fairbanks, R., and Bönisch, G.. (1994). Arctic river-runoff: mean residence time on the shelves and in the halocline. *Deep Sea Res. Part I: Oceanographic Res. Papers* 41, 1053–1068. doi: 10.1016/0967-0637(94)90018-3

Schuler, K. H., and Tortell, P. D. (2023). Impacts of vertical mixing and ice-melt on N2O and CH4 concentrations in the Canadian Arctic Ocean. *Continental Shelf Res.* 269, 105124. doi: 10.1016/j.csr.2023.105124

Seitzinger, S., Harrison, J. A., Böhlke, J. K., Bouwman, A. F., Lowrance, R., Peterson, B., et al. (2006). Denitrification across landscapes and waterscapes: a synthesis. *Ecol. Applications: A Publ. Ecol. Soc. America* 16, 2064–2090. doi: 10.1890/1051-0761(2006)016[2064:dalawa]2.0.co;2

Sheng, Y., Smith, L. C., MacDonald, G. M., Kremenetski, K. V., Frey, K. E., Velichko, A. A., et al. (2004). A high-resolution GIS-based inventory of the west Siberian peat carbon pool. *Global Biogeochemical Cycles* 18, GB3004. doi: 10.1029/2003GB002190

Smith, L. C., MacDonald, G. M., Velichko, A. A., Beilman, D. W., Borisova, O. K., Frey, K. E., et al. (2004). Siberian peatlands a net carbon sink and global methane source since the early Holocene. *Sci. (New York N.Y.)* 303, 353–356. doi: 10.1126/science.1090553

Sun, X., Humborg, C., Mörth, C.-M., and Brüchert, V. (2021). The importance of benthic nutrient fluxes in supporting primary production in the laptev and east siberian shelf seas. *Global Biogeochemical Cycles* 35, e2020GB006849. doi: 10.1029/2020GB006849

Tang, W., Ward, B. B., Beman, M., Bristow, L., Clark, D., Fawcett, S., et al. (2023). Database of nitrification and nitrifiers in the global ocean. *Earth System Sci. Data* 15, 5039–5077. doi: 10.5194/essd-15-5039-2023

Terhaar, J., Lauerwald, R., Regnier, P., Gruber, N., and Bopp, L. (2021). Around one third of current Arctic Ocean primary production sustained by rivers and coastal erosion. *Nat. Commun.* 12, 169. doi: 10.1038/s41467-020-20470-z

Thurnherr, I., Moallemi, A., and Makhotin, M. (2024). Flow-distortion corrected meteorological measurements from the Arctic century expedition in August/September 2021. *ETH Zurich*. doi: 10.3929/ethz-b-000693692

Tian, H., Xu, R., Canadell, J. G., Thompson, R. L., Winiwarter, W., Suntharalingam, P., et al. (2020). A comprehensive quantification of global nitrous oxide sources and sinks. *Nature* 586, 248–256. doi: 10.1038/s41586-020-2780-0

Tian, H., Pan, N., Thompson, R. L., Canadell, J. G., Suntharalingam, P., Regnier, P., et al. (2024). Global nitrous oxide budget, (1980-2020). *Earth System Sci. Data* 16, 2543–2604. doi: 10.5194/essd-16-2543-2024

Toyoda, S., Kakimoto, T., Kudo, K., Yoshida, N., Sasano, D., Kosugi, N., et al. (2021). Distribution and production mechanisms of N2O in the western arctic ocean. *Global Biogeochemical Cycles* 35, e2020GB006881. doi: 10.1029/2020GB006881

Tremblay, J.-É., Anderson, L. G., Matrai, P., Coupel, P., Bélanger, S., Michel, C., et al. (2015). Global and regional drivers of nutrient supply, primary production and CO2 drawdown in the changing Arctic Ocean. *Prog. Oceanography* 139, 171–196. doi: 10.1016/j.pocean.2015.08.009

Upstill-Goddard, R. C., Rees, A. P., and Owens, N. J. P. (1996). Simultaneous high-precision measurements of methane and nitrous oxide in water and seawater by single phase equilibration gas chromatography. *Deep Sea Res. Part I: Oceanographic Res. Papers* 43, 1669–1682. doi: 10.1016/S0967-0637(96)00074-X

National Oceanic and Atmospheric Administration (NOAA), n.d. (2024). *Global Monitoring Laboratory (GML)*. Available online at: https://gml.noaa.gov/ (Accessed June 11, 2024).

Verdugo, J., Damm, E., Snoeijs, P., Díez, B., and Farías, L. (2016). Climate relevant trace gases (N2O and CH4) in the Eurasian Basin (Arctic Ocean). *Deep Sea Res. Part I: Oceanographic Res. Papers* 117, 84–94. doi: 10.1016/j.dsr.2016.08.016

Wanninkhof, R. (2014). Relationship between wind speed and gas exchange over the ocean revisited. *Limnology Oceanography: Methods* 12, 351–362. doi: 10.4319/lom.2014.12.351

Ward, B. B. (2008). "Chapter 5 - nitrification in marine systems," in *Nitrogen in the marine environment, 2nd*. Ed. D. G. Capone, D. A. Bronk, M. R. Mulholland and E. J. Carpenter (Academic Press, San Diego), 199–261. doi: 10.1016/B978-0-12-372522-6.00005-0

Weiss, R. F. (1981). Determinations of carbon dioxide and methane by dual catalyst flame ionization chromatography and nitrous oxide by electron capture chromatography. *J. Chromatographic Sci.* 19, 611–616. doi: 10.1093/chromsci/19.12.611

Weiss, R. F., and Price, B. A. (1980). Nitrous oxide solubility in water and seawater. *Mar. Chem.* 8, 347–359. doi: 10.1016/0304-4203(80)90024-9

Wild, B., Ray, N. E., Lett, C., Davies, A.J., Kirillova, E., Holmstrand, H., et al. (2023). Nitrous oxide dynamics in the siberian arctic ocean and vulnerability to climate change. *J. Geophysical Research: Biogeosciences* 128, e2022JG007326. doi: 10.1029/2022JG007326

Wu, M., Chen, L., Zhan, L., Zhang, J., Li, Y., and Liu, J. (2017). Spatial variability and factors influencing the air-sea N2O flux in the bering sea, chukchi sea and chukchi abyssal plain. *Atmosphere* 8, 65. doi: 10.3390/atmos8040065

Yang, S., Chang, B.X., Warner, M.J., Weber, T.S., Bourbonnais, A.M., Santoro, A.E., et al. (2020). Global reconstruction reduces the uncertainty of oceanic nitrous oxide emissions and reveals a vigorous seasonal cycle. *Proc. Natl. Acad. Sci.* 117, 11954–11960. doi: 10.1073/pnas.1921914117

Zhan, L., Chen, L., Zhang, J., and Li, Y. (2015). A vertical gradient of nitrous oxide below the subsurface of the Canada Basin and its formation mechanisms. *J. Geophysical Research: Oceans* 120, 2401–2411. doi: 10.1002/2014JC010337

Zhan, L., Chen, L., Zhang, J., Yan, J., Li, Y., and Wu, M. (2016). A permanent N2O sink in the Nordic Seas and its strength and possible variability over the past four decades. *J. Geophysical Research: Oceans* 121, 5608–5621. doi: 10.1002/2016JC011925

Zhan, L., Wu, M., Chen, L., Zhang, J., Li, Y., and Liu, J. (2017). The air-sea nitrous oxide flux along cruise tracks to the arctic ocean and southern ocean. *Atmosphere* 8, 216. doi: 10.3390/atmos8110216

Zhan, L., Zhang, J., Ouyang, Z., Lei, R., Xu, S., Qi, D., et al. (2021). High-resolution distribution pattern of surface water nitrous oxide along a cruise track from the Okhotsk Sea to the western Arctic Ocean. *Limnology Oceanography* 66, S401–S410. doi: 10.1002/lno.11604

Zhang, J., Zhan, L., Chen, L., Li, Y., and Chen, J. (2015). Coexistence of nitrous oxide undersaturation and oversaturation in the surface and subsurface of the western Arctic Ocean. *J. Geophysical Research: Oceans* 120, 8392–8401. doi: 10.1002/2015JC011245